Available online at www.sciencedirect.com
ScienceDirect
International Journal of Heat and Mass Transfer 50 (2007) 3376–3389
International Journal of HEAT and MASS TRANSFER
www.elsevier.com/locate/ijhmt

Local current density and water management in PEMFCs

Dewan Hasan Ahmed, Hyung Jin Sung *

Department of Mechanical Engineering, Korea Advanced Institute of Science and Technology, 373-1, Guseong-dong Yuseong-gu, Daejeon 305-701, South Korea

Received 17 February 2006; received in revised form 12 October 2006

Abstract

We have used computational fluid dynamics analysis to investigate the local current density distribution at the membrane-gas diffusion layer (GDL) interface at average current densities ranging from 0.1 to 2.4 A/cm^2. A three-dimensional, non-isothermal model was used with a single straight channel geometry. Both anode and cathode humidification were included in the model. In addition, phase transportation was included in the model to predict the distributions of water vapor and liquid water and the related water management for systems operating at different current densities. The dependency of local current density on total water and thermal management of the fuel cell and its other related linkage with physical parameters were investigated. The simulation results showed that at low average current density, the local current density does not vary along the width but gradually decreases along the cell length. However, the opposite trend starts to emerge as the average current density is increased. The anode water activity was found to play a significant role in determining the membrane conductivity and the local current density variation in the cell. Moreover, at high average current density, the local current density in the downstream end of the channel is dominated by the cathode water rather than the membrane conductivity. Specifically, the cathode water accumulates in the shoulder area and congests the pores of the GDL, thereby blocking the passage of oxygen to the reacting area. The resulting scarcity of oxygen in the shoulder area causes a dramatic reduction in the local current density in this region. Simulations using different cathode stoichiometric rates showed that increasing the cathode stoichiometric rate led to better oxygen transportation to the GDL at the shoulder area, and hence improved to smooth the local current density distribution. The model was validated by comparison with the polarization curve (I–V characteristics) in the literature.

1. Introduction

Proton exchange membrane fuel cells (PEMFCs) have been a topic of intense research interest for several decades. During this time, researchers have developed an understanding of the mechanism and operational complexities of PEMFCs. Nowadays, PEMFCs are a promising type of fuel cell in the automobile industry with numerous advantages, including high power density, low emission, low temperature and low noise. In recent years, numerical modeling and simulation techniques have been widely used to study different aspects of PEMFCs with a view to enhancing cell performance. Among the various factors that determine PEMFC performance, the management of water, which plays a vital role in determining the membrane conductivity, is the most intricate. Too much or too little water in the cell will lead to disturb reactants supply or to increase ionic resistance, respectively, and thus reduce the overall performance of the fuel cell. The main method used to characterize fuel cell performance across different average current density ranges is to examine polarization curves; however, the local current density distribution in the fuel cell can expose the real water and thermal management along with other features to enhance the cell performance. Computational fluid dynamics techniques can be used to determine the local current density distribution and its dependence on water and thermal management.

Water and thermal management in PEMFCs has been studied using one- to three-dimensional mathematical

* Corresponding author. Tel.: +82 42 869 3027; fax: +82 42 869 5027.
E-mail address: hjsung@kaist.ac.kr (H.J. Sung).

0017-9310/$ - see front matter © 2007 Elsevier Ltd. All rights reserved.
doi:10.1016/j.ijheatmasstransfer.2007.01.056

Nomenclature

A_{cv}	specific surface area of the control volume, m^{-1}
$Area_{cv}$	surface area of the control volume, m^2
C_{wa}	concentration of water vapor at the anode, mol/m^3
C_{wc}	concentration of water vapor at the cathode, mol/m^3
$D_{H_2,l}$	diffusion coefficient of H_2 in a liquid water film, 6.3×10^{-9} m^2/s
$D_{O_2,l}$	diffusion coefficient of O_2 in a liquid water film, 2.4×10^{-9} m^2/s
D_W	diffusion coefficient of water, m^2/s
F	Faraday constant, 96487 C/mol
$H_{H_2,l}$	Henry's law constant for H_2 in a liquid water film, 8.9×10^9 Pa
$H_{O_2,l}$	Henry's law constant for O_2 in a liquid water film, 2.12×10^{10} Pa
h	enthalpy, kJ/kg
h_{rxn}	enthalpy of water formation, kJ/Kmol
h_{fg}	enthalpy of vaporization of water, kJ/kg
I	local current density, A/m^2
I_{avg}	average current density, A/m^2
$I_{o,K}$	exchange current density for reaction K, A/m^2
k	thermal conductivity, W/m K
L	length, m
$M_{m,dry}$	equivalent weight of a dry membrane, kg/mol
M_n	molecular weight of species n, kg/mol
m_n	mass fraction of species n
$m_{w,l}$	mass fraction of liquid water
$mass_n$	mass of species n, kg
n_d	electro-osmosis drag coefficient
$P^{sat}_{w,k}$	saturation vapor pressure of water in stream k, Pa
P	pressure, Pa
P_n	partial pressure of species n, Pa
R	universal gas constant, 8.314 J/mol K
r	condensation rate, 1/s
S	source term
t_f	liquid water film thickness, m
t_m	membrane thickness, m
T	temperature, K
V_{OC}	open circuit voltage, V
V_{cell}	cell voltage, V
W	width, m
$X_{i,k}$	mole fraction of species i in stream k

Greek symbols

α	net water flux per proton
β	permeability, m^2
ε	porosity of the gas diffusion layer
η	overpotential, V
λ	water content in the membrane
μ	dynamic viscosity, kg s/m^2
$\rho_{m,dry}$	density of a dry membrane, kg/m^3
ρ	density of the mixture, kg/m^3
σ_m	membrane conductivity, S/m

Subscripts and superscripts

a	anode
c	cathode
cv	control volume
e	electrochemical reaction
glif	gas liquid interface
H_2	hydrogen
K	anode or cathode
l	liquid
O_2	oxygen
sat	saturated
v	vapor
ξ	dummy variable for direction x, y or z

models and numerical simulations. However, most studies performed to date were focused on water formation, distribution and overall performance of the fuel cell with global polarization curve. Springer et al. [1] and Bernardi and Verbrugge [2] were the first researchers to devise a mathematical model for fuel cells. Their fuel cell model was restricted to one-dimensional and isothermal processes. Later, Fuller and Newman [3] and Nguyen and White [4] developed a two-dimensional model for PEMFCs that could handle non-isothermal cases. Indeed, their findings gave researchers a basic understanding of water and thermal management in PEMFCs. In formulating their models, however, they ignored various issues such as humidification, condensation of water vapor, and the presence of a gas diffusion layer. Subsequently, numerous studies were carried out on various aspects of PEMFCs using two-dimensional [5,6] and three-dimensional [7–11] models; these studies yielded a more detailed understanding of water and thermal management in PEMFCs. However, none the model used in these studies accounted for the impact of anode–cathode humidification on condensation of water vapor. Shimpalee and Dutta [12] extended the works of Dutta et al. [11] to include phase transformation. Most of the above studies were carried out with the aim of generating a global understanding of the polarization curve under different boundary conditions with regard to water management rather than the local current density distribution with its related local water and thermal management.

In recent years, a small number of research papers have appeared concerning the local current density distribution in PEMFCs. Dutta et al. [11] studied the local current density distribution on the membrane surface using a three-dimensional model with water management. They found that the local current density distribution was not uniform

along the channel or across the width. The key point revealed by their research was that water transportation between the anode and cathode channels had a major effect on the current density distribution. Specifically, water migration from the anode to the cathode leads to a higher current density at the reacting area than at the channel area. However, their model was isothermal and did not account for the phase transformation between water vapor and liquid water. Berning et al. [13] reported that the local current density is always higher in the channel area than in the shoulder area. In their model, they assumed that the activation overpotential was constant over the catalyst interface. Later, Nguyen et al. [14] extended the computational models of Berning et al. [13] to allow variations in the activation overpotential. Using this extended model, they found that the current density at a local area depends on oxygen mass transport to that area. At high average current density, the shoulder area experiences lower current density due to a lack of oxygen. Recently, Sivertsen and Djilali [15] conducted computer modeling of PEMFC including electric and ionic potential transport. They found that the local current density profile correlates with the activation overpotential, but not with the oxygen concentration, and that the ohmic losses are larger in the areas of the catalyst layer under the flow channels. Further, they showed that higher electronic conductivity reduces the ohmic losses, causing concentration losses to dominate and the local current density to be reduced. However, the above three studies of the local current density did not consider phase transformation or the presence of liquid water. Natarajan and Nguyen [16,17] found using two- and three-dimensional models that the performance of the cathode is dominated by the dynamics of liquid water, especially at high current densities. They further reported that the local current density at the reacting area above the shoulder is lower than that at the reacting area above the channel, and that the current density along the length is directly affected by oxygen availability. However, inlet humidification was not considered in their model. Meng and Wang [18] also investigated the local current distribution in the cell, using a three-dimensional isothermal model. They observed that at low average current density, the local current density is predominantly determined by the electronic conductivity. Oxygen concentration plays an important role at high average current density. However, there is no evidence made in their paper regarding oxygen concentration or water management for local current density variations at high average current density. Using a two-dimensional isothermal model, Sun et al. [19,20] determined the local current density variation along the width for different channel-width ratios. They found that the maximum reaction rate shifts from under the land or shoulder to the flow channel depending on the total overpotential. However, they ignored the water activity and did not consider water accumulation in the membrane-gas diffusion layer (GDL) and catalyst layer. It is clear from the literature that the local current density varies in the cell, and that several factors may contribute to these variations. However, there remains a need for a clear understanding of water management and its effects on the local current density distribution and also the behavior of reactants at different average current densities.

The objective of the present study was to investigate the local current density distribution in cells operating at different average current densities. The investigation encompassed low, medium, moderately high, and high average current densities and the related water management in the cell. Particular emphasis was placed on the relationships between local current density and water management, reactant flow behavior in the cell, and related issues. A three-dimensional model with a single straight channel geometry was used for the numerical simulations. The local flow behaviors of the reactants in the cell and their effects on local water transportation were examined. The membrane conductivity, water activity, overpotential and temperature of the cell were analyzed in detail in regard to the overall cell performance for systems with different average current densities. In addition, to analyze the details of the local current density variation in PEMFCs, the investigation was further extended to include different cathode stoichiometric rates.

2. Numerical simulation

Schematic diagram of the computational domain and its cross sectional view are shown in Fig. 1. The system consists of two channels (for hydrogen and air) between which the membrane electrode assembly (MEA) is sandwiched. There are bipolar plates on both the anode and cathode sides, which function as current collectors with high electronic conductivity. Humidified hydrogen and air are introduced into the respective channels where the quantities of the two gases are determined by the stoichiometric rate and average current density. The flow is considered to be laminar and steady state flow. The governing equations for the numerical simulation are conservation of mass, momentum transport, species transport and energy equations.

Conservation of mass equation

$$\nabla \cdot (\rho \vec{u}) = S_{m_a} + S_{m_c} \tag{1}$$

The source terms are

$$S_{m_a} = S_{H_2} + S_{wv_p} + S_{wl_p} + S_{awv_e} \quad \text{at } z = z_3, \tag{1.1}$$

$$S_{m_c} = S_{O_2} + S_{wv_p} + S_{wl_p} + S_{cwv_e} \quad \text{at } z = z_2, \tag{1.2}$$

where

$$S_{H_2} = -\frac{M_{H_2} A_{cv} I}{2F} \quad \text{at } z = z_3, \quad \text{and}$$

$$S_{O_2} = -\frac{M_{O_2} A_{cv} I}{4F} \quad \text{at } z = z_2. \tag{1.3}$$

The mass contributions of the water vapor at the anode and cathode sides are

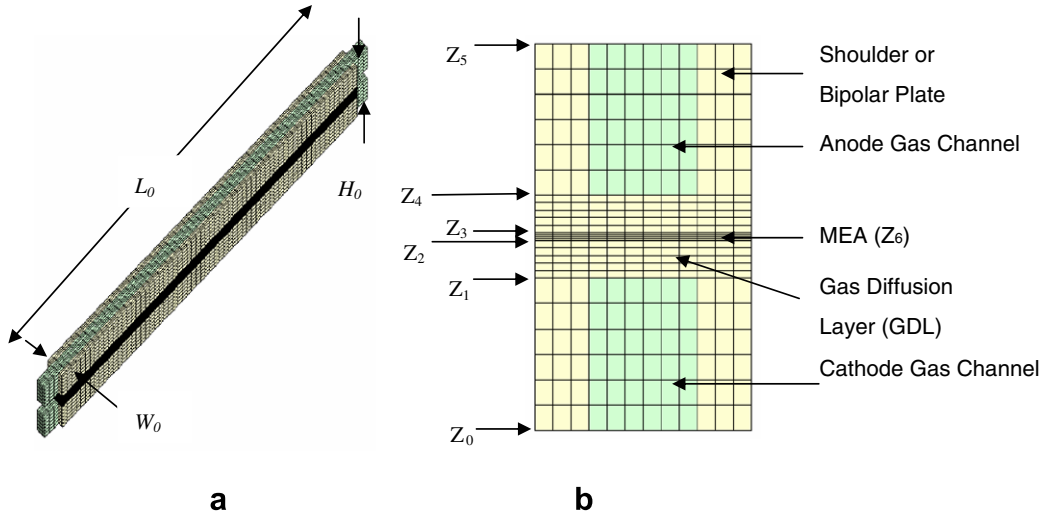

Fig. 1. Single straight channel flow field for a PEMFC. (a) Geometry, (b) cross sectional view.

$$S_{\mathrm{awv_e}} = -\frac{M_{\mathrm{H_2O}} A_{\mathrm{cv}} \alpha I}{F} \quad \text{at } z = z_3, \tag{1.4}$$

$$S_{\mathrm{cwv_e}} = S_{\mathrm{cwv_p}} + S_{\mathrm{cwv_t}} = \frac{M_{\mathrm{H_2O}} A_{\mathrm{cv}} I}{2F} + \frac{\alpha M_{\mathrm{H_2O}} A_{\mathrm{cv}} I}{F} = \frac{(1+2\alpha) M_{\mathrm{H_2O}} A_{\mathrm{cv}} I}{2F} \quad \text{at } z = z_2. \tag{1.5}$$

The change of phases between water vapor and liquid water depends on the partial pressure, and is defined as [12]

$$S_{\mathrm{wl_p}} = -S_{\mathrm{wv_p}} = -\frac{M_{\mathrm{H_2O}} \sum_{n \text{ of v}} \frac{\mathrm{mass}_{n \text{ of v}}}{M_{n of v}}}{\left(1 - \frac{P_{\mathrm{wv}}^{\mathrm{sat}}}{P}\right)} \left[\frac{P_{\mathrm{wv}}^{\mathrm{sat}} - P_{\mathrm{wv}}}{P}\right] * r \quad \text{at } z_0 \leqslant z \leqslant z_5. \tag{1.6}$$

In Eqs. (1.3)–(1.5), α is the net water transfer coefficient per proton

$$\alpha = n_{\mathrm{d}} - \frac{F D_{\mathrm{W}} [C_{\mathrm{wc}} - C_{\mathrm{wa}}]}{I t_{\mathrm{m}}}. \tag{1.7}$$

The electro-osmotic drag coefficient (n_{d}) and water diffusion coefficient (D_{W}) can be correlated with membrane water content (λ) [1],

$$n_{\mathrm{d}} = 0.0029\lambda^2 + 0.05\lambda - 3.4 \times 10^{-19}. \tag{1.8}$$

Momentum transport equation

$$\nabla \cdot (\rho \vec{u} \vec{u}) = -\nabla P + \nabla \cdot (\mu \nabla \vec{u}) + S_{\mathrm{p},i}, \tag{2}$$

where $S_{\mathrm{p},i}$ is the sink source term for porous media in the x, y and z directions

$$S_{\mathrm{p},i} = -\frac{\mu u_i}{\beta_i} \quad \text{at } z_1 \leqslant z \leqslant z_2 \quad \text{and} \quad z_3 \leqslant z \leqslant z_4. \tag{2.1}$$

Here, β is the permeability.

General species transport equation

$$\nabla \cdot (\rho m_n \vec{u}) = \nabla \cdot (J_n) + S_{\mathrm{s}}. \tag{3}$$

Here n denotes H_2, O_2, water vapor or liquid water. The source terms are the same as those for the conservation of mass equation. The transportation of the species is solved with bulk mixture velocities and with diffusion mass fluxes. The diffusion mass flux of each species is evaluated with binary diffusion coefficients [21], which are reduced by 50% in the diffusion layer to account for the effect of porosity and tortuosity of the pores [11]. In the present model, it is assumed that the liquid water is in small droplet forms and freely suspended in the gas flow. This allows us to consider a two-phase flow together (homogeneous two-phase flow) rather than the two phase flow with different velocities found in literature [22]. This assumption does not allow us to operate the PEMFC at supersaturated conditions with high loading liquid water for steady state operation. The diffusion mass flux (J) of species n in direction ξ is

$$J_{\xi,n} = -\rho D_{\xi,n} \frac{\partial m_{\mathrm{K},n}}{\partial \xi}, \tag{3.1}$$

where ξ is a dummy variable for direction x, y or z.

Energy equation

$$\nabla (\rho \vec{u} h) = \nabla \cdot (k \nabla T) + S_{\mathrm{h}}. \tag{4}$$

The source term S_{h} will have contributions from energy losses and heat associated with phase transformations. The heat source from the electrochemical reaction is given by the difference of the total energy released by the electrochemical reaction at the cathode membrane surface and the electrical energy extracted out of the fuel cell [23]

$$S_{\mathrm{h_e}} = h_{\mathrm{rxn}} \left[\frac{I A_{\mathrm{cv}}}{2F}\right]_{z=z_2} - (I V_{\mathrm{cell}} A_{\mathrm{cv}})_{z=z_2} \quad \text{at } z = z_6, \tag{4.1}$$

The heat source due to a phase change

$$S_{\mathrm{h_p}} = S_{\mathrm{wl_p}} * h_{\mathrm{fg}} \quad \text{at } z_0 \leqslant z \leqslant z_5, \tag{4.2}$$

where h_{fg} is the enthalpy of formation of water. The local current density of the cell is calculated from the open circuit voltage (V_{OC}) and the losses

$$I = \frac{\sigma_{\mathrm{m}}}{t_{\mathrm{m}}} \{V_{\mathrm{OC}} - V_{\mathrm{cell}} - \eta\}, \tag{5}$$

where t_m is the membrane thickness and σ_m is the membrane conductivity, both of which are calculated as functions of the water content on the membrane surface at the anode interface. The membrane conductivity can be defined as [4,7,11]

$$\sigma_m = \left(0.514\frac{M_{m,dry}}{\rho_{m,dry}}C_{wa} - 0.326\right)\exp\left(1268\left(\frac{1}{T_0}-\frac{1}{T}\right)\right), \tag{6}$$

where $T_0 = 303$ K. The water vapor concentration is defined as

$$C_{wa} = \frac{\rho_{m,dry}}{M_{m,dry}}\lambda, \tag{7}$$

where $\rho_{m,dry}$ and $M_{m,dry}$ are the material density and the equivalent weight of a dry membrane, respectively. The water content in the membrane (λ) is defined as

$$\begin{aligned} &\lambda = (0.043 + 17.8a_K - 39.8a_K^2 + 36.0a_K^3), \quad \text{if } a_K \leqslant 1 \\ &\lambda = (14 + 1.4(a_K - 1)), \quad \text{if } a_K > 1. \end{aligned} \tag{8}$$

The subscript K stands for anode or cathode. a_a is the water activity and defined as

$$a_a = \frac{X_{w,a}P}{P_{w,a}^{sat}}, \tag{9}$$

where P is the cell pressure and $X_{w,a}$ is the mole fraction of water on anode side.

The local overpotential for a PEMFC can be written as [12]

$$\eta = \frac{RT}{\alpha_c F}\ln\left[\frac{IP}{I_{0_{O_2}}P_{0_{O_2}}}\right] + \frac{RT}{\alpha_a F}\ln\left[\frac{IP}{I_{0_{H_2}}P_{0_{H_2}}}\right], \tag{10}$$

where P is the pressure and P_0 is the partial pressure of the reactants, α_a and α_c are the transfer coefficients for anode and cathode respectively, and I_0 is the exchange current density. The partial pressure is calculated as $P_{O_2} = X_{O_2}P$, and $P_{H_2} = X_{H_2}P$.

In the present model, the source terms of different conservation equations correspond to the control volume, not to the boundary conditions of anode or cathode interface. To determine the concentration and the activities at the membrane-GDL interface correctly, the mole fraction of each species is extrapolated to the membrane surface. The exception is made when the liquid water film is generated on the membrane surface. If the liquid water is present at MEA, the model accounts for the mass transfer resistance of the gas diffusing through the film. In such case, Henry's Law is used to calculate the solubility of reactants in the liquid water film [23]. The diffusion length of this soluble gas is determined by the thickness of the film of water on MEA corrected for the porosity of the GDL. Moreover, it accounts for the average pore flooding by considering an average film thickness.

$$\begin{aligned} -\frac{I}{4F}M_{O_2} &= \rho_{O_2}D_{O_2,l}\left[\frac{X_{O_2,glif}P_{glif}H_{O_2,l}^{-1} - X_{O_2}}{t_{f,c}}\right] \quad \text{at } z = z_2, \\ -\frac{I}{2F}M_{H_2} &= \rho_{H_2}D_{H_2,l}\left[\frac{X_{H_2,glif}P_{glif}H_{H_2,l}^{-1} - X_{H_2}}{t_{f,a}}\right] \quad \text{at } z = z_3, \end{aligned} \tag{11}$$

where P_{glif} is the pressure at the gas–liquid water interface, H is the Henry constant of the reactants in the liquid water film, and $t_{f,K}$ is the liquid water film thickness for the anode and cathode, which is defined as

$$t_{f,K} = \frac{m_{w,l}(\sum \text{mass}_n)}{\varepsilon\rho_{wl}\text{Area}_{cv}}. \tag{12}$$

Here, ε is the porosity of the gas diffusion layer, $m_{w,l}$ is the liquid water mass fraction at membrane-GDL interface and mass_n is the mass of species n. The geometrical and physical parameters are listed in Tables 1 and 2, respectively. The above all governing equations and appropriate boundary conditions are solved by using the user coding capabilities of STAR-CD that employ a finite volume method.

Table 1
Geometrical parameters

Parameter	Value (mm)
Channel length	34.7
Channel width	1
Channel height	1
Membrane length	31.7
Membrane thickness	0.05
Anode gas diffusion layer	0.25
Cathode gas diffusion layer	0.25

Table 2
Physical and electrochemical parameters

Parameter	Value	Value [11]
Anode pressure	1 atm	1 atm
Cathode pressure	1 atm	1 atm
Stoichiometric rate at anode	1.2	2.0
Stoichiometric rate at cathode	2.0	2.0
Cell temperature	70 °C	70 °C
Anode inlet temperature	80 °C	80 °C
Cathode inlet temperature	70 °C	80 °C
Open circuit voltage	0.96 V	1.1 V
Relative humidity at anode	100%	100%
Relative humidity at cathode	100%	0%
Oxygen inlet mole fraction	0.143	1.0
Oxygen exchange current density	200 A/m^2	100 A/m^2
Hydrogen exchange current density	2000 A/m^2	1000 A/m^2
Anode transfer coefficient	1.2	1.0
Cathode transfer coefficient	0.6	0.5
Porosity	0.7	0.7
Permeability	1×10^{-12} m^2	2×10^{-10} m^2
Thermal conductivity of bipolar plate [24]	5.7 W/m K	5.7 W/m K
Thermal conductivity of GDL [24]	0.213 W/m K	0.213 W/m K
Thermal conductivity of MEA [24]	0.147 W/m K	0.147 W/m K

3. Results and discussion

Before proceeding further, it is important to first establish the reliability of our simulation results. To achieve this, we ran our model using the physical parameters listed in Table 2, and compared the resulting polarization curve with that obtained by Dutta et al. [11] using similar physical parameters (see Table 2). As shown in Fig. 2, the two polarization curves exhibit similar trends, but are displaced with respect to each other by an almost constant voltage difference. This constant displacement can be attributed to differences in the physical parameters used, specifically the open circuit voltage, exchange current density, transfer coefficient, permeability, reactant inlet boundary conditions, and so on. In general, the reactants flow rate depends on average current density of the cell and their transportations are greatly affected by the produced water, in such consequence, the local current density distribution may vary through out the cell. In this study, five average current densities, ranging from low to very high (0.1, 0.6, 1.0, 1.6 and 2.4 A/cm^2), were chosen and the local current density distribution at the membrane-GDL interface was examined for each of these average current densities. Related issues, including water management, thermal management, and other fluid dynamic and electrochemical aspects are also considered.

The present simulation results show that, at low average current density ($I_{avg} = 0.1$ A/cm^2), the local current density (I) varies along the channel length but is almost uniform along the width (see Fig. 3a). On increasing the average current density (I_{avg}), however, the reverse trend (i.e., variation along the width and uniform along the channel) starts to emerge. At high average current density ($I_{avg} = 1.6$ A/cm^2), the local current density is slightly decreased along the channel but there is more variation along the width (see Fig. 3b). In addition, at high I_{avg} the local current density is lower at the reacting area over the channel (channel area) and higher at the reacting area over the shoulder (shoulder area). With moving downstream in the channel, however, the local current density at the shoulder gradually decreases.

The local current density variations along the width for various I_{avg} values at $L/L_0 = 0.957$ are shown in Fig. 4. For low I_{avg}, the local current density is almost uniform along the width. As I_{avg} is increased, however, maxima in the local current density appear and shift towards the shoulder areas. For very high I_{avg} ($I_{avg} = 2.4$ A/cm^2), the maxima in the local current density coincide with the shoulder–channel interface. Moreover, for very high I_{avg}, away from the channel, the local current density plummets at the shoulder area.

The local current density directly depends on various parameters, and many other parameters affect its distribution over the cell. According to Eq. (5), the local current density is directly related to the local overpotential and membrane conductivity. An increase in the local overpotential in the cell gives rise to a decrease in the local current density. On the other hand, the local current density increases with increasing membrane conductivity. In these systems, the local overpotential is the result of contributions from both the anode and cathode, referred to as the anode overpotential and cathode overpotential respectively. These overpotentials, in turn, represent both activation and concentration losses. It is well established that the magnitude of the anode overpotential is much less than that of the cathode overpotential, and that the major losses occur at the cathode side [25].

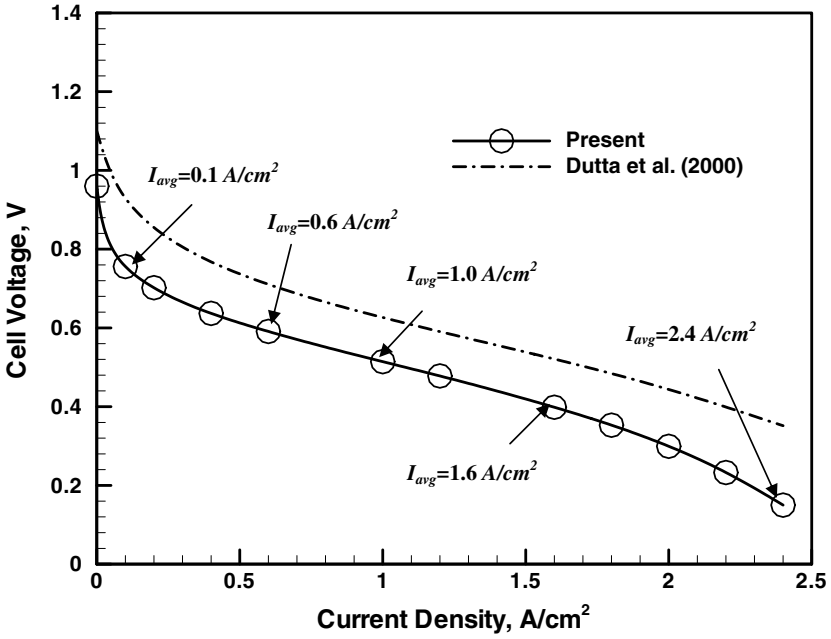

Fig. 2. Polarization curve.

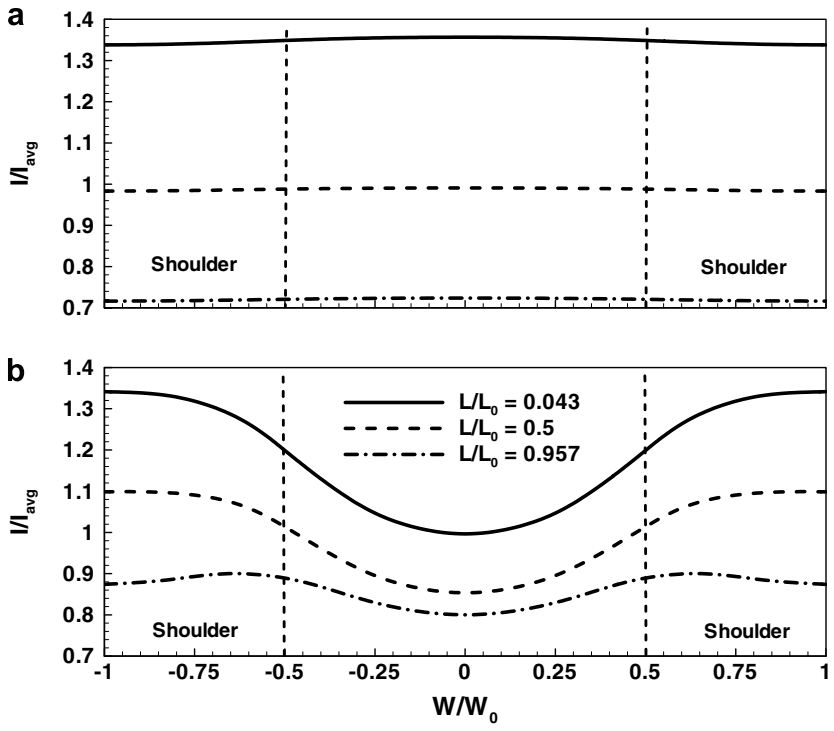

Fig. 3. Non-dimensionlaized local current density distribution at the membrane-cathode GDL interface. (a) $I_{avg} = 0.1$ A/cm^2 and (b) $I_{avg} = 1.6$ A/cm^2.

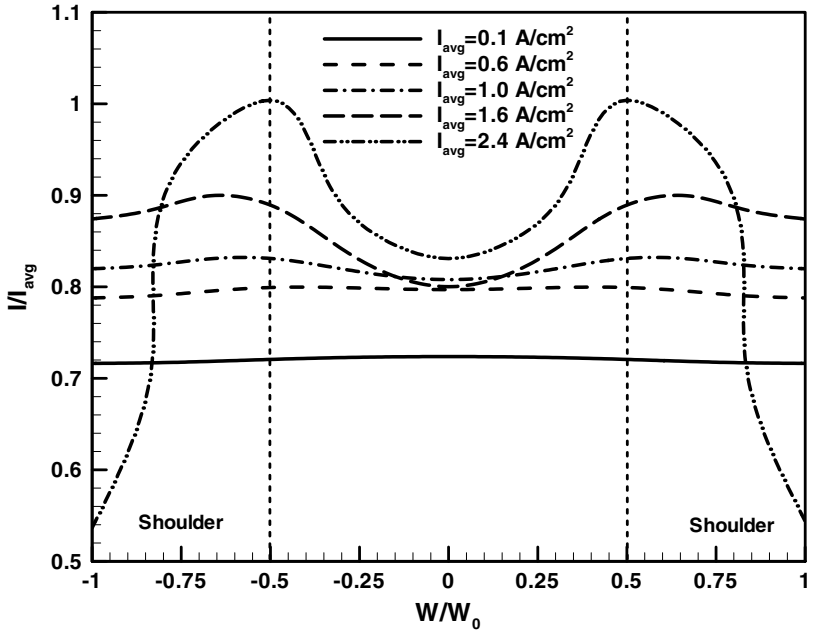

Fig. 4. Non-dimensionalized local current density distribution at the membrane-cathode GDL interface, $L/L_0 = 0.957$.

Fig. 5 shows a comparison of the anode and cathode overpotentials for an average current density of 1.6 A/cm^2. The anode overpotential at the membrane-GDL interface (Fig. 5a) shows a trend similar to that observed in the local current density (Fig. 3b). By contrast, the cathode overpotential increases along both the length and width. Consistent with previous findings, the anode overpotential is much less than the cathode overpotential, and should have little effect on the local current density. The local overpotential (Eq. (7)) is calculated from the Butler–Volmer equation including reactant partial pressures for concentration losses and activation losses. However, the local overpotential is inter-related with local current density, reactants partial pressure and total pressure of the cell (Eqs. (5) and (7)). Fig. 6 shows the reactant mole fraction distributions along the width and at different channel

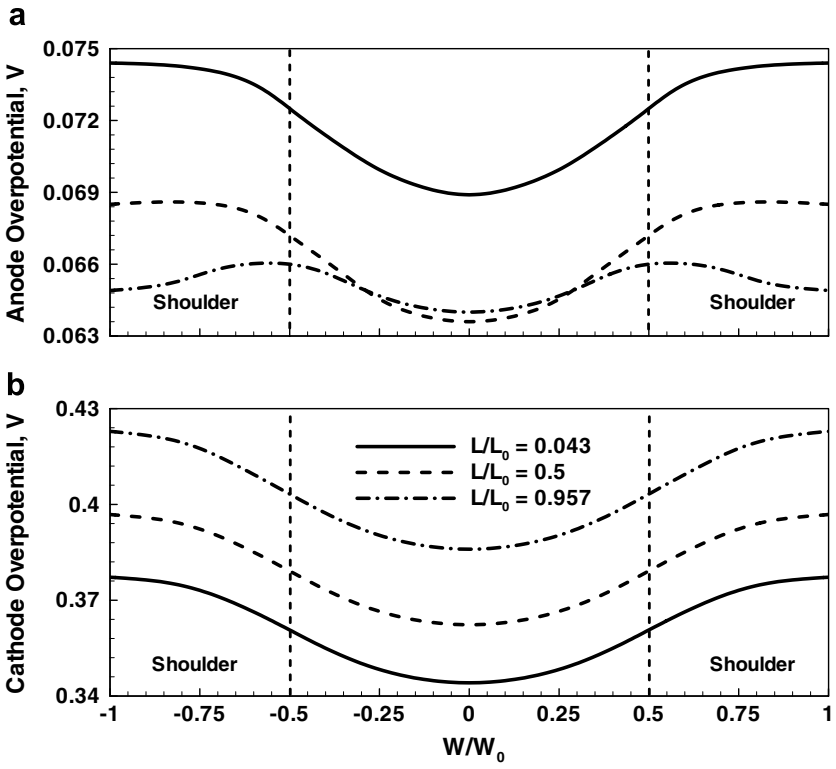

Fig. 5. Local overpotential distribution at the membrane-GDL interface for $I_{avg} = 1.6$ A/cm^2. (a) anode overpotential and (b) cathode overpotential.

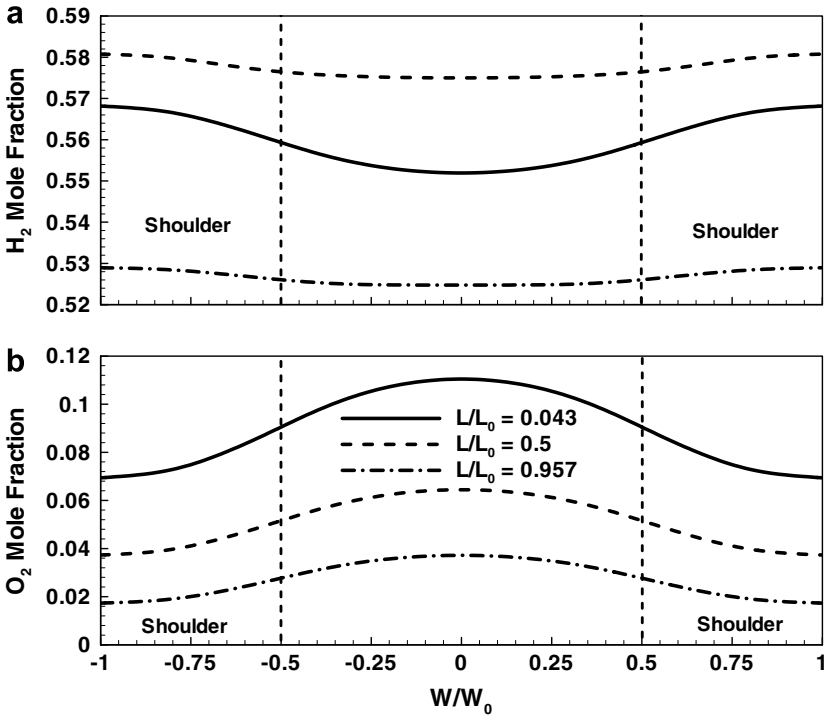

Fig. 6. Reactant distribution at the membrane-GDL interface for $I_{avg} = 1.6$ A/cm^2. (a) H_2 and (b) O_2.

lengths for an average current density of 1.6 A/cm^2. The hydrogen mole fraction (Fig. 6a) is slightly higher in the shoulder area than in the channel area, whereas the oxygen mole fraction (Fig. 6b) is much lower in the shoulder area than in the channel area. The reactants distributions show their greatest influence on overpotential in the cell especially on the cathode side as the major losses occur at the cathode side [25]. Sivertsen and Djilali [15] reported that

the current density distribution depends on the activation overpotential distribution in the cell, as they found that the ohmic losses in the GDL influence the catalyst activity rather than the concentration losses. As a result, they mentioned that the current density profile in the cell resembled the cathode activation overpotential distribution. However, they did not consider the phase transformation between water vapor and liquid water. In fact, a higher overpotential leads to a lower overall current density in the cell. In PEMFC, the small magnitude of the anode overpotential compared to the cathode overpotential, we believe that the anode overpotential is not a significant determinant of the local current density distribution in the reacting area. By contrast, the cathode overpotential likely has a large effect on the local current density distribution in the cell due to reactant concentration losses and activation losses. Moreover, water management also regulates the mass transportation of the reactants to the reacting area, especially at high I_{avg}.

The variation in the oxygen mole fraction along the width is much more pronounced than that of the hydrogen mole fraction. Water formation at the cathode and water transportation from anode to cathode by electro-osmosis create conditions that act to lower the oxygen mole fraction in the shoulder area. In these systems, the transportation of water between anode and cathode along the channel and the phase transformation from water vapor to liquid water vary depending on the operating current density range and are also important determinants of the reactant flow distribution in the cell [26]. In the present study, we have examined whether local current density variations in PEMFCs can be explained through analysis of the total water management as a function of the average current density.

The local current density depends on the local membrane conductivity (Eq. (5)), which in turn is strongly influenced by the anode water concentration and the cell temperature (Eq. (6)). The anode water concentration depends on the anode water activity. Increasing the anode water activity or the cell temperature increases the local membrane conductivity. However, increasing the temperature also causes a rapid increase in the water saturation pressure, which leads to a decrease in the water activity. In addition to these effects, the presence of water at the anode (fully humidified hydrogen) channel serves to increase the anode water activity. As a result, the total water and thermal management in the fuel cell regulates the local membrane conductivity.

Figs. 7 and 8 show the anode water activity and temperature distribution at the membrane-anode GDL interface for two average current densities, $I_{avg} = 0.1$ and 1.6 A/cm^2. At low average current density ($I_{avg} = 0.1$ A/cm^2), the anode water activity (Fig. 7a) is almost uniform along the width. However, the water activity decreases in the downstream region and then remains constant until the exit. Compared to the behavior at low current density, at high current density ($I_{avg} = 1.6$ A/cm^2) the anode water activity varies much more strongly along both the channel length and width (Fig. 7b), with the activity being higher at the reacting area over the shoulder than in the channel center. The corresponding temperature distributions, shown in Fig. 8, show quite different trends. At both low and high current density, the temperature is higher at the reacting

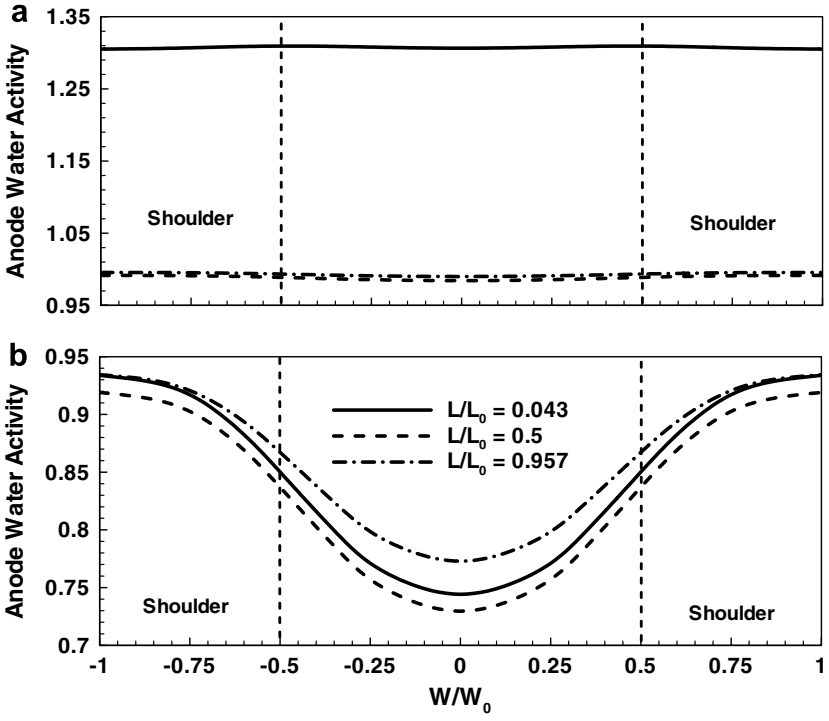

Fig. 7. Anode water activity at the membrane-anode GDL interface. (a) $I_{avg} = 0.1$ A/cm^2 and (b) $I_{avg} = 1.6$ A/cm^2.

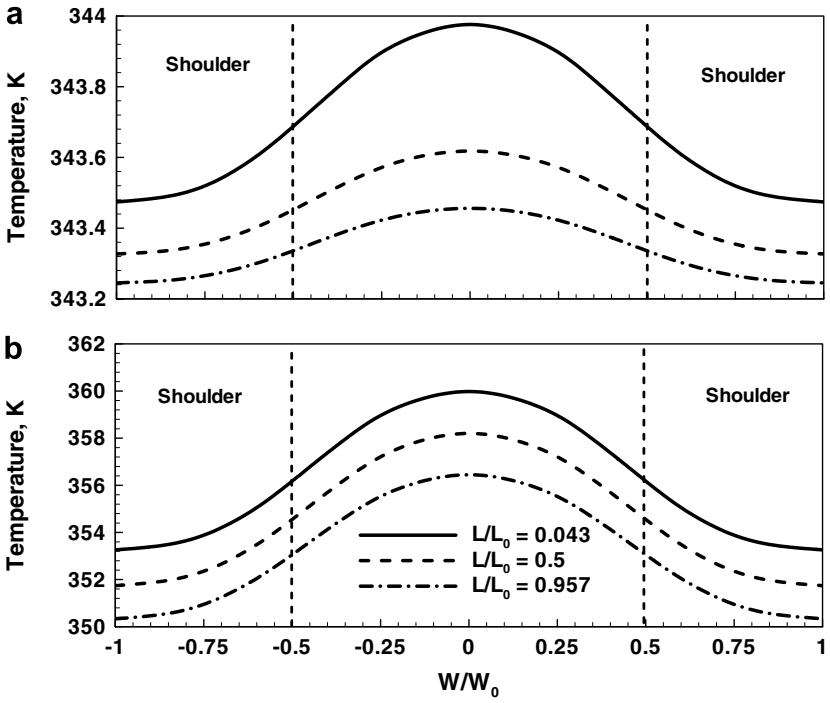

Fig. 8. Local temperature at membrane-anode GDL interface. (a) $I_{avg} = 0.1$ A/cm^2 and (b) $I_{avg} = 1.6$ A/cm^2.

area over the channel (or channel area) and lower at the shoulder area, although the difference in temperature between the channel and shoulder areas is much greater at high current density. It is noteworthy that the temperature variation along the length and width at low current density ($I_{avg} = 0.1$ A/cm^2) is significantly lower than that observed at high average current density ($I_{avg} = 1.6$ A/cm^2). The total scenario of anode water activity can be seen in the plots of the water vapor mole fraction at the anode side, shown in Fig. 9. At low average current density, the water vapor mole fraction remains almost constant along the width (Fig. 9a); however, the relatively small temperature variation across

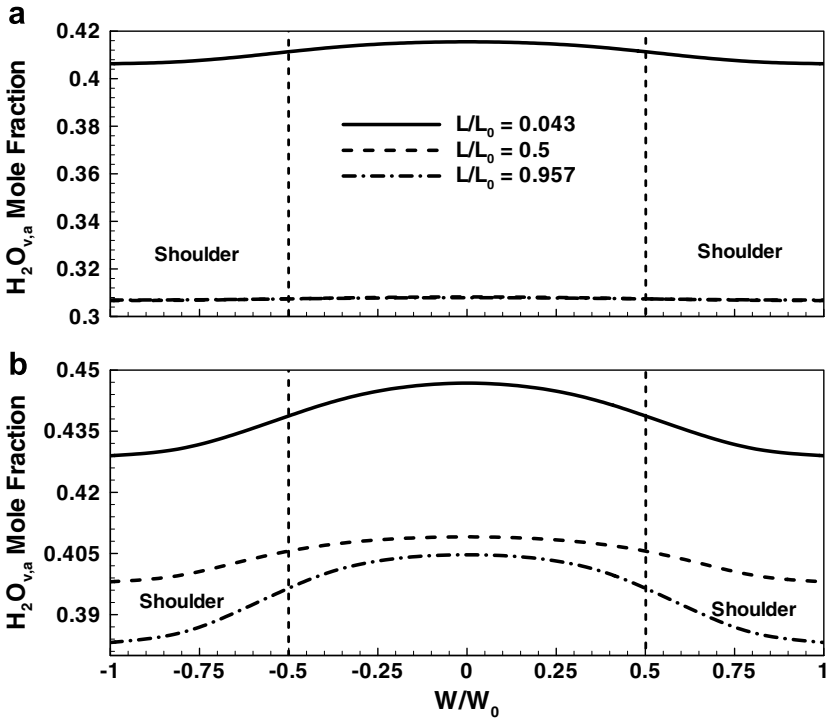

Fig. 9. Anode water vapor mole fraction at the membrane-anode GDL interface. (a) $I_{avg} = 0.1$ A/cm^2 and (b) $I_{avg} = 1.6$ A/cm^2.

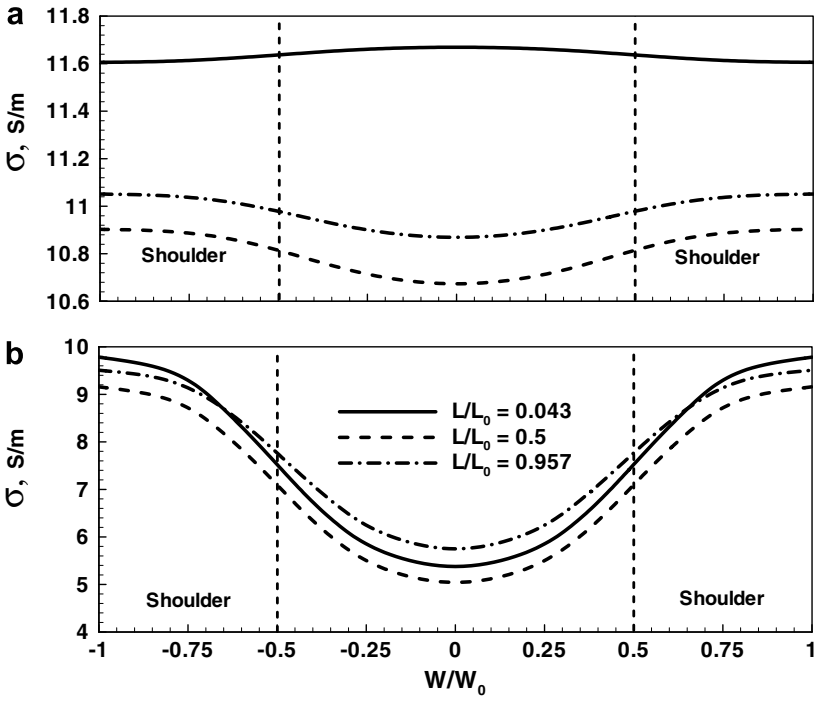

Fig. 10. Local membrane conductivity at the membrane-GDL interface. (a) $I_{avg} = 0.1$ A/cm^2 and (b) $I_{avg} = 1.6$ A/cm^2.

the width at low average current density (Fig. 8a) means that the water activity remains approximately constant (Fig. 7a). At high average current density, by contrast, the higher temperature variation along the width (6–7 K) causes the water activity to be higher at the shoulder area than in the channel area (see Fig. 7b).

As discussed above, the conductivity of the membrane is directly related to the anode water activity. Consistent with this, the variations in membrane conductivity along the channel and width (Fig. 10) resemble those observed for the anode water activity. Specifically, at low average current density the membrane conductivity is higher at the inlet region and decreases in the downstream region; and at high average current density, the membrane conductivity is higher in the shoulder area and lower in the channel area. Indeed, the overall membrane conductivity decreases on going from low to high average current density (compare Fig. 10a and b). This trend in the membrane conductivity comes from the combined effects of the variations in the anode water activity and temperature along the width [27]. Comparing Figs. 3 and 10, we see that the local current density follows the trend of the local membrane conductivity. Note that the local current density at the shoulder area near the exit does not follow the same trend. Especially at high average current density, the local current density decreases along the channel at the shoulder area. As a result, the maximum local current density is shifted towards the shoulder–channel interface. This prompted us to further investigate the relation between the local current density and reactant distributions in the PEMFC.

As shown in Fig. 6, oxygen is depleted both with moving downstream along the channel and with moving out along the width from the channel center. The important issue is that the scarcity of oxygen at shoulder area is not compensated by the higher membrane conductivity in this area. Several factors could explain the scarcity of oxygen in the shoulder region. Usually, greater amounts of water are produced at the cathode side through electrochemical reactions. This (liquid) water congests the pores of the GDL, blocking the passage of oxygen to the reacting area. Another factor that could potentially lead to a scarcity of oxygen is the oxygen (air) flow rate, which may be lower for these particular reactions in the downstream end of the cathode channel. The mole fractions of water vapor and liquid water at the cathode side at high average current density (1.6 A/cm^2) are shown in Fig. 11. The data show an accumulation of both liquid and vapor water in the shoulder area, which will block the passage of oxygen to the reacting area above the shoulder. Natarajan and Nguyen [17] showed that liquid water over the channel area is rapidly removed from that region than the shoulder area because of the shorter diffusion distance along the diffusion layer thickness. Moreover, water is generated at the shoulder area and accumulates over this area. As a result, the shoulder area is always saturated with water despite the lower rate of water generation in that region.

Lower current density at the shoulder area and the related oxygen scarcity on that region insists us to carry further simulations with different cathode stoichiometric rates for different average current densities. Fig. 12 shows the local current density distribution along the width at $L/L_0 = 0.957$ for average current densities of $I_{avg} = 1.6$ and 2.4 A/cm^2. As the cathode stoichiometric rate increases, the local current density at the shoulder area

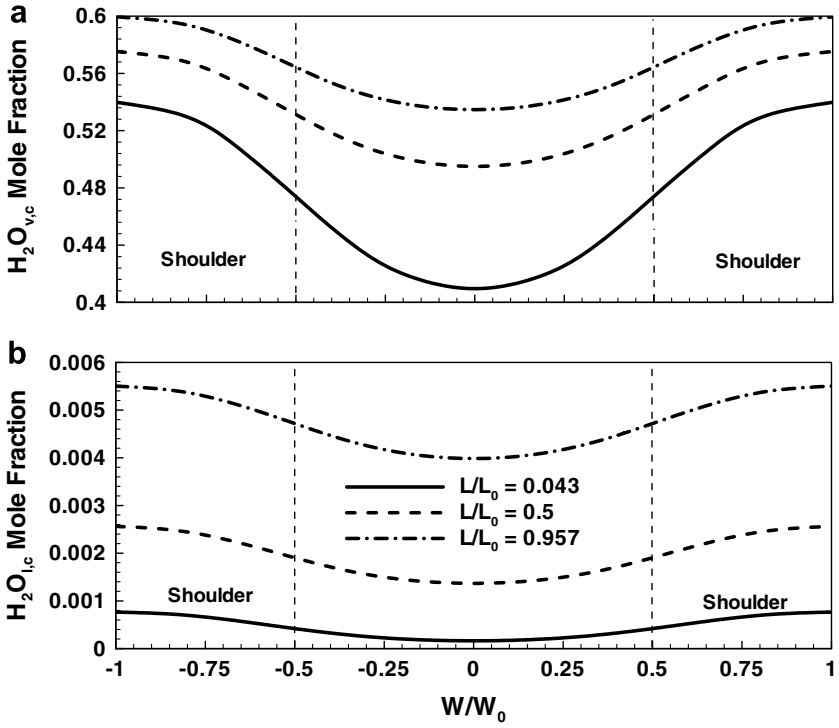

Fig. 11. Cathode water distribution at the membrane-cathode GDL interface for $I_{avg} = 1.6$ A/cm^2. (a) Water vapor and (b) liquid water.

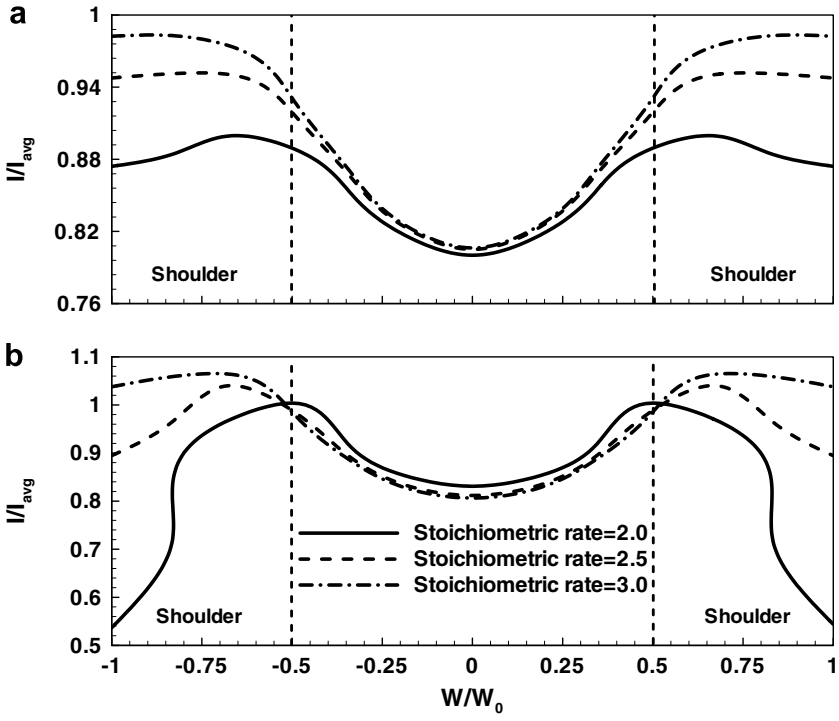

Fig. 12. Non-dimensionalized local current density distribution at the membrane-cathode GDL interface, $L/L_0 = 0.957$. (a) $I_{avg} = 1.6$ A/cm^2 and (b) $I_{avg} = 2.4$ A/cm^2.

increases. Further evidence of improved local current density at the shoulder area is found by examining the corresponding distributions of the oxygen mole fraction (Fig. 13), which show that the oxygen mole fraction at the shoulder area increases with increasing cathode stoichiometric rate.

Besides with the reactants distribution, water distribution on both anode and cathode side plays major role on

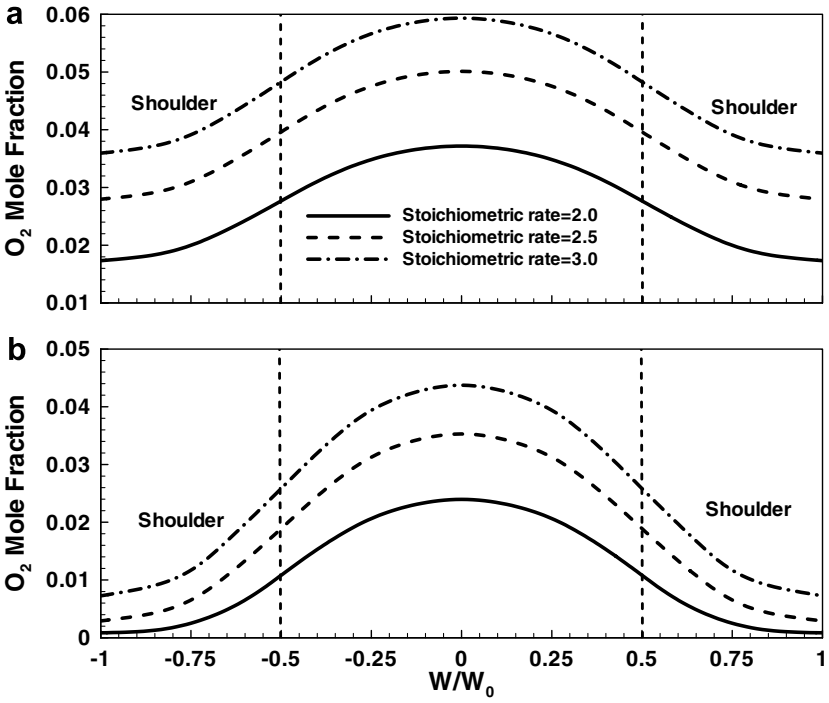

Fig. 13. Oxygen mole fraction at the membrane-cathode GDL interface, $L/L_0 = 0.957$. (a) $I_{avg} = 1.6$ A/cm^2 and (b) $I_{avg} = 2.4$ A/cm^2.

cell performance especially at high current density operation. Cathode side water creates obstacle for proper oxygen distribution and in anode side, the anode water activity and temperature play very important roles in PEMFCs, especially for local current density distribution. The importance of these variables in anode side arises because they both strongly influence the final membrane conductivity in the cell. We found that the membrane conductivity is higher in the shoulder area and lower in the channel area, which leads to a similar trend in the local current density. Our simulation results also showed that the profile of the anode overpotential along the width is also similar to that of the local current density; however, the magnitude of the anode overpotential is much lower than that of the cathode overpotential, and hence has much less effect on the local current density distribution. Our data additionally indicated that water activity plays a main role in determining the local current distribution. Moreover, we found that water at the cathode side plays an additional vital role in the downstream region of the channel: it tends to accumulate in the shoulder area and congests the pores of the GDL, thereby blocking the passage of oxygen to the reacting area. However, the local current density distribution in the shoulder area could be improved by increasing the cathode stoichiometric rate.

4. Summary and conclusions

In the present study, we have carried out simulations of a PMEFC using a single straight channel geometry and including both anode and cathode humidification. The main aim of this work was to examine the local current density behavior in the cell and its dependence on water and thermal management. First, we calculated the local current density profile along both the channel length and width for a range of average current densities. The simulation results showed that at low average current densities, the local current density varied along the length of the channel but was much more uniform along its width. As the average current density was increased, however, the profile started to change to the opposite shape, such that at high average current density, the local current density gradually decreased along the channel and showed substantial variation along its width. We found that the profile of the anode overpotential along the width resembled the local current density profile. However, the magnitude of the anode overpotential was much less than that of the cathode overpotential. Water activity and local temperature played major roles in determining the membrane conductivity, and moreover, directly affected the local current density distribution. In addition, the simulation data indicated that water in the cathode side of the cell played a vital role in determining the local current density distribution in the downstream region of the channel. Specifically, on the cathode side water accumulated in the shoulder area, where it congested the pores of the GDL. As a result, there was a lack of oxygen in the GDL, leading to concentration losses and an increased cathode overpotential. Investigations using different cathode stoichiometric rates showed that increasing the cathode stoichiometric rate can improve the local current density distribution, especially at high average current densities.

Acknowledgement

This work was supported by the Brain Korea 21 Project in 2007.

References

[1] T.E. Springer, T.A. Zawodzinski, S. Gottesfeld, Polymer electrolyte fuel cell model, J. Electrochem. Soc. 138 (8) (1991) 2334–2342.
[2] D.M. Bernardi, M.W. Verbrugge, A mathematical model of the solid-polymer-electrolyte fuel cell, J. Electrochem. Soc. 139 (9) (1992) 2477–2491.
[3] T.F. Fuller, J. Newman, Water and thermal management in solid-polymer-electrolyte fuel cells, J. Electrochem. Soc. 140 (5) (1993) 1218–1225.
[4] T.V. Nguyen, R.E. White, A water and heat management model for proton-exchange-membrane fuel cells, J. Electrochem. Soc. 140 (8) (1993) 2178–2186.
[5] K. Dannenberg, P. Ekdunge, G. Lindbergh, Mathematical model of the PEMFC, J. Appl. Electrochem. 30 (2000) 1377–1387.
[6] V. Garau, H. Liu, S. Kakac, Two-dimensional model for proton exchange membrane fuel cells, AIChE J. 44 (11) (1998) 2410–2422.
[7] S. Dutta, S. Shimpalee, J.W. Van Zee, Numerical prediction of mass-exchange between cathode and anode channel in a PEM fuel cell, Int. J. Heat Mass Trans. 44 (2001) 2029–2042.
[8] S. Um, C.Y. Wang, K.S. Chen, Computational fluid dynamics modeling of proton exchange membrane fuel cells, J. Electrochem. Soc. 147 (12) (2000) 4485–4493.
[9] S. Um, C.Y. Wang, Three-dimensional analysis of transport and electrochemical reactions in polymer electrolyte fuel cells, J. Power Sources 125 (2004) 40–51.
[10] K.W. Lum, J.J. McGuirk, Three-dimensional model of a complete polymer electrolyte membrane fuel cell – model formulation, validation and parametric studies, J. Power Sources 143 (2005) 103–124.
[11] S. Dutta, S. Shimpalee, J.W. Van Zee, Three-dimensional numerical simulation of straight channel PEM fuel cells, J. Appl. Electrochem. 30 (2000) 135–146.
[12] S. Shimpalee, S. Dutta, Numerical prediction of temperature distribution in PEM fuel cells, Numer. Heat Trans. Part A 38 (2000) 111–128.
[13] T. Berning, D.M. Lu, N. Djilali, Three-dimensional computational analysis of transport phenomena in a PEM fuel cell, J. Power Sources 106 (2002) 284–294.
[14] P.T. Nguyen, T. Berning, N. Djilali, Computational model of PEM fuel cell with serpentine gas flow channels, J. Power Sources 130 (2004) 149–157.
[15] B.R. Sivertsen, N. Djilali, CFD-based modelling of proton exchange membrane fuel cells, J. Power Sources 141 (2005) 65–78.
[16] D. Natarajan, T.V. Nguyen, Three-dimensional effects of liquid water flooding in the cathode of a PEM fuel cell, J. Power Sources 115 (2003) 66–80.
[17] D. Natarajan, T.V. Nguyen, A two-dimensional, two-phase, multi-component, transient model for the cathode of a proton exchange membrane fuel cell using conventional gas distributors, J. Electrochem. Soc. 148 (12) (2001) A1324–A1335.
[18] H. Meng, C.Y. Wang, Electron transport in PEFCs, J. Electrochem. Soc. 151 (3) (2004) A358–A367.
[19] W. Sun, B.A. Peppley, K. Karan, An improved two-dimensional agglomerate cathode model to study the influence of catalyst layer structural parameters, Electrochem. Acta 50 (2005) 3359–3374.
[20] W. Sun, B.A. Peppley, K. Karan, Modeling of influence of GDL and flow-field plate parameters on the reaction distribution in the PEMFC cathode catalyst layer, J. Power Sources 144 (2005) 42–53.
[21] J.C. Slattery, R.B. Bird, Calculation of the diffusion coefficient of dilute gases and of the self-diffusion coefficient of dense gases, AIChE J. 4 (1958) 137–142.
[22] L. You, H. Liu, A two-phase flow and transport model for the cathode of PEM fuel cells, Int. J. Heat Mass Trans. 45 (2002) 2277–2287.
[23] STAR-CD Version 3.24 Methodology, CD-Adapco Group.
[24] S. Shimpalee, S. Geenway, D. Spuckler, J.W. Van Zee, Predicting water and current distributions in a commercial-size PEMFC, J. Power Sources 135 (2004) 79–87.
[25] J. Larminie, A. Dicks, Fuel Cell Systems Explained, Second ed., Wiley, England, 2003, pp. 51–52.
[26] D.H. Ahmed, H.J. Sung, J. Bae, D.R. Lee, Reactants flow behavior and water management for different current densities in PEMFC, J. Heat Mass Trans., submitted for publication.
[27] D.H. Ahmed, H.J. Sung, Effects of channel geometrical configuration and shoulder width on PEMFC performance at high current density, J. Power Sources 162 (2006) 327–339.